JOURNAL OF BACTERIOLOGY, Apr. 2011, p. 1718–1725 Vol. 193, No. 7
0021-9193/11/$12.00 doi:10.1128/JB.01395-10

Structural and Mechanical Properties of *Klebsiella pneumoniae* Type 3 Fimbriae▽§

Feng-Jung Chen,[1,2]† Chia-Han Chan,[1]† Ying-Jung Huang,[3] Kuo-Liang Liu,[4] Hwei-Ling Peng,[3] Hwan-You Chang,[5] Gunn-Guang Liou,[7] Tri-Rung Yew,[4] Cheng-Hsien Liu,[6] Ken Y. Hsu,[2] and Long Hsu[1]*

Institute and Department of Electrophysics,[1] Department of Photonics and Institute of Electro-Optical Engineering,[2] and Department of Biological Science and Technology,[3] National Chiao Tung University, 1001 University Road, Hsinchu 300, Taiwan, Republic of China; Department of Materials Science and Engineering,[4] Institute of Molecular Medicine and Department of Life Sciences,[5] and Department of Power Mechanical Engineering,[6] National Tsing Hua University, 101, Section 2, Kuang-Fu Road, Hsinchu 300, Taiwan, Republic of China; and Division of Molecular and Genomic Medicine, National Health Research Institutes, 35 Keyan Road, Jhunan, Miaoli County 350, Taiwan, Republic of China[7]

Received 22 November 2010/Accepted 6 January 2011

This study investigated the structural and mechanical properties of *Klebsiella pneumoniae* type 3 fimbriae, which constitute a known virulence factor for the bacterium. Transmission electron microscopy and optical tweezers were used to understand the ability of the bacterium to survive flushes. An individual *K. pneumoniae* type 3 fimbria exhibited a helix-like structure with a pitch of 4.1 nm and a three-phase force-extension curve. The fimbria was first nonlinearly stretched with increasing force. Then, it started to uncoil and extended several micrometers at a fixed force of 66 ± 4 pN ($n = 22$). Finally, the extension of the fimbria shifted to the third phase, with a characteristic force of 102 ± 9 pN ($n = 14$) at the inflection point. Compared with the P fimbriae and type 1 fimbriae of uropathogenic *Escherichia coli*, *K. pneumoniae* type 3 fimbriae have a larger pitch in the helix-like structure and stronger uncoiling and characteristic forces.

Adhesion of many pathogenic bacteria to host cells is a critical step in initiating infections. Bacterial fimbriae, hair-like appendages expressed on bacterial surfaces, play an important role in mediating the adhesion process of many bacterial species (26). For example, P-type fimbriae and type 1 fimbriae are essential to the ability of uropathogenic *Escherichia coli* to cause urinary tract infections (37). Similarly, type 3 fimbriae have been demonstrated to assist *Klebsiella pneumoniae* in causing respiratory tract infections (21).

The bacterial adhesion must be sufficiently strong to resist drag forces arising from aqueous flushes in the urethra or gaseous flushes in the respiratory tract. Fimbriae exhibiting flexible and stretchable properties similar to that of springs may aid bacteria in remaining attached to host cells by reducing the impact of the flushes. This assumption has been examined and verified only for P fimbriae and type 1 fimbriae from structural and biomechanical points of view in the past 2 decades (6, 17, 24, 29). An individual P-type or type 1 fimbria is approximately 7 nm in diameter and 1 to 2 μm in length (6, 34, 35). Adhesin molecules are located at the distal end of the fimbria for host cell attachment, while pilins are assembled into a three-dimensional helical structure to form the fimbrial backbone (12, 30, 38). The helical structure may enable the fimbriae to stretch and, as a result, enable the bacteria to resist being flushed away.

The mechanical elasticity of *E. coli* P fimbriae was first determined experimentally with optical tweezers (OT) in 2004 (16, 24). The force-extension curve (FEC) of a single P fimbria can be divided into three phases (Fig. 1). In the first phase, a fimbria behaves like a Hooke's spring and extends in direct proportion to the increasing force that results from an average Young's modulus of 4 MPa (10^6 pN/μm^2). As the stretching force approaches 28 pN, the FEC of the fimbria switches dramatically from the first phase to the second phase and the fimbria is stretched up to a few micrometers at this fixed force. The particular force is referred to as the uncoiling force (F_{uc}) of P fimbriae because the uncoiling of adjacent spiral coils of the helical fimbria successively takes place in the second phase. After the helical structure of the fimbria is fully uncoiled to a thin filament, the FEC shifts to the third phase and is characterized by an S shape. In this phase, another particular stretching force of the fimbria occurs at the inflection point (x_c) of the S-shaped FEC, where the slope is minimal. This particular force is denoted the characteristic force (F_{ch}), which for P fimbriae is 67 pN (1).

The mechanical elasticity of *E. coli* type 1 fimbriae was subsequently determined with atomic force microscopy (17, 29) and OT (2). As schematically shown in Fig. 1, individual type 1 fimbriae also exhibit three-phase FECs. The uncoiling and characteristic forces of type 1 fimbriae are 30 pN and 67 pN, respectively, which are comparable with those of P fimbriae. In contrast, the physiological impact of a urine flush on individual bacteria was measured to be ~90 pN/bacterium in

* Corresponding author. Mailing address: Institute and Department of Electrophysics, National Chiao Tung University, 1001 University Road, Hsinchu 300, Taiwan, Republic of China. Phone: (886) 3-5712121, ext. 56161. Fax: (886) 3-5131241. E-mail: long@cc.nctu.edu.tw.

† These authors contributed equally to this work.

§ Supplemental material for this article may be found at http://jb.asm.org/.

▽ Published ahead of print on 14 January 2011.

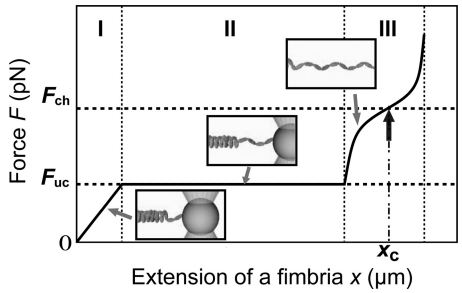

FIG. 1. Typical force-extension curve of a P fimbria (24) or a type 1 fimbria (2). The force-extension curve is divided into three phases. Furthermore, x_c, depicted by the black arrow, is the length at which the slope has a minimum value in phase III. The uncoiling force in phase II is denoted by F_{uc}, and the characteristic force at x_c in phase III is denoted by F_{ch}. For P fimbriae, the uncoiling force is 28 pN and the characteristic force is 67 pN. In addition, for type 1 fimbriae, the uncoiling force is 30 pN and the characteristic force is also 67 pN. Three insets are representations of a fimbria stretched by optical tweezers in each of the three phases (at the points indicated by gray arrows), respectively.

flow chamber experiments (42). The impact is strong enough to trigger the extension of type 1 fimbriae and, therefore, causes uropathogenic *E. coli* organisms to dangle from the epithelial cells in the urinary tract. Recently, the *E. coli* S fimbriae, which are also capable of binding to human bladder and kidney epithelia, were shown to exert weaker layer-to-layer (LL) bonds than both P fimbriae and type 1 fimbriae (9). Nevertheless, these results undoubtedly support the finding that stretchable fimbriae are essential to reducing the force due to urine flow and ensuring a successful attachment for uropathogenic bacteria in urinary tract infections. With a different adhesion strategy, the coil-like T4 fimbriae were also shown to have a large degree of flexibility in order to sustain external forces (8).

K. pneumoniae is a common nosocomial pathogen causing both pneumonia and urinary tract infections. Furthermore, *K. pneumoniae* is one of the major causes of liver abscesses, especially in patients with diabetes mellitus (43). Most pathogenic *K. pneumoniae* strains produce type 3 fimbriae, which are critical for bacterial biofilm formation (31, 39). Although the mouse model has failed to establish an association of type 3 fimbriae with lung or urinary tract infections, type 3 fimbriae have been implicated in having an accessory role in urinary tract infections (39). In addition, type 3 fimbriae have been demonstrated to mediate bacterial attachments to several cell types, including tracheal epithelial cells, renal tubular cells, extracellular matrix proteins, and components of basement membranes of human lung tissue (21, 40, 41). Like uropathogenic *E. coli*, *K. pneumoniae* is subject to the impact of flushes at the sites of infection, such as the respiratory tract and renal tubes, although the forces are likely to be different from those experienced by uropathogenic *E. coli* in the urinary tract.

We previously characterized the adhesive component MrkD of type 3 fimbriae (22) and also measured the adhesion forces of type 3 fimbriae to type IV collagen with OT (10). In this study, we further characterize the structural and mechanical properties of *K. pneumoniae* type 3 fimbriae with transmission electron microscopy (TEM) and OT, respectively. The fine structure of the fimbriae was analyzed with TEM images, and their persistence length and Young's modulus were further estimated with an additional method, statistical polymer chain analysis (33). In addition, the FEC of a single type 3 fimbria was determined with OT. The differences between type 3 and other types of fimbriae with respect to their structural and mechanical properties and the implications of bacterial adherence to host cells are also discussed.

MATERIALS AND METHODS

Bacterial culture. Type 3-fimbria-expressing *E. coli* JM109(p*mrkABCD*) was grown in Luria-Bertani (LB) broth supplemented with 100 μg/ml ampicillin at 37°C for 20 h with shaking. The bacteria in LB medium were directly used for TEM analysis. For elasticity experiments, bacteria were centrifuged for 1 min at 9,000 × *g*, washed twice with phosphate-buffered saline (PBS; 137 mM NaCl, 2.7 mM KCl, 10 mM Na_2HPO_4, and 2 mM KH_2PO_4), and then resuspended in PBS for later use.

Sample preparation for transmission electron microscopy. Preparation of bacterial samples for TEM analysis has been described elsewhere (28). Briefly, a 200-mesh copper grid covered with carbon-coated collodion film was glow discharged for 1 min. Next, 2.5 μl of freshly resuspended *E. coli* in LB medium was adsorbed to the discharged grid, washed with 3 drops of distilled water, and stained with 2 drops of 2% (wt/vol) uranyl acetate.

The TEM images of *E. coli* were inspected with a Tecnai G^2 Spirit TWIN (FEI Company, Hillsboro, OR) and operated at an acceleration voltage of 120 kV with a defocus value of −131.76 nm. The images were recorded at two magnifications, ×2,380 and ×67,000. The micrographs were digitized with a Zeiss imaging scanner (Z/I Imaging Corporation, Huntsville, AL) to form 5,786- by 7,143-pixel 12-bit images, with a raster of 2.15 Å/pixel.

Statistical polymer chain analysis. The flexibility of a polymer is usually quantified as a persistence length. The persistence length has the dimensions of length. Here, a polymer is regarded as flexible when its persistence length is comparable to or smaller than the segment of interest. Conversely, the persistence length of a rigid polymer is many times longer than the segment of interest. Persistence lengths (P) were calculated for ~1,200 segments of 600 fimbriae from 50 electron micrographs, using the relationship (5, 33)

$$\langle R^2 \rangle = 4PL \times \left(1 - \frac{2P}{L} \times (1 - e^{-L/2P})\right) \quad (1)$$

where R is the end-to-end distance of a filament segment and L is the contour length of the segment. The expected values of R^2 for the morphology of each segment were derived from frequency histograms (see Fig. 4B and C).

For thermal bending of flexible polymers, as occurs with fimbriae in two-dimensional equilibrium, the persistence length is given by the equation (32)

$$P = (E \times I)/(k \times T) \quad (2)$$

where E is Young's modulus of elasticity, I is the geometric moment of inertia, k is Boltzmann's constant, and T is temperature. Using the measured geometry of a type 3 fimbria, the Young's modulus of the fimbriae was calculated from the persistence length with equation 2. The geometric moment of inertia (I) of the filaments is equal to $(\pi/4)\,(D_a \times D_i/4)^2$, where D_a and D_i are the largest diameter and the smallest diameter on elliptic cross sections of a fimbria.

Image processing and structural analysis. All images were processed using two commercial software packages, Photoshop (Adobe Systems, Inc., San Jose, CA) and AutoCAD (Autodesk, Inc., San Rafael, CA). Photoshop was used to cut 506 subpictures (1,715 by 436 pixels in area) from 50 raw pictures (5,786 by 7,143 pixels in area). Then, these cut pictures were loaded into AutoCAD to measure structural parameters and end-to-end distances of a type 3 fimbria. All measured parameters were in units of pixels before being converted to a real size. In the studies of the structural parameters, we estimated unstretched lengths, pitches, and widths of a fimbria. In the studies of Young's moduli, we estimated expected values of end-to-end distances ($\langle R \rangle$) of fimbrial segments first. The details of the estimating process are described in Supplement 3 in the supplemental material. Next, substituting values for $\langle R \rangle$ in equation 1 resulted in persistence lengths (P). Finally, we estimated the Young's moduli (E) of a type 3 fimbria by substituting values for P in equation 2.

Sample preparation for optical tweezers. Protein A latex beads (1 μm in diameter; Polysciences, Inc., Warrington, PA) previously washed with protein A/G buffer (0.1 M Tris-HCl, 0.15 M NaCl) were incubated with anti-MrkD antibody at 4°C for 1 h. After incubation, the beads coated with anti-MrkD antibody were washed with protein A/G buffer again, resuspended in PBS, and

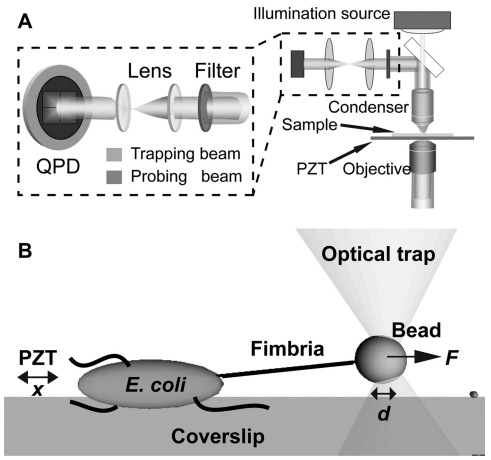

FIG. 2. (A) Schematic illustration of our force-measuring optical tweezers system. A trapping laser beam and a probing laser beam are guided into an inverted microscope and then passed through a high-numerical-aperture objective to form two diffraction-limited focal points on a sample. The trapping laser can be used to capture a particle in three dimensions. The probing laser can be used to detect force-dependent displacements of the trapped particle with a quadrant photodiode (QPD). PZT, piezoelectric stage. (B) Sketch of the measurement procedure. A bacterium is immobilized on a coverslip. Several type 3 fimbriae adhere to a surface-modified bead in the optical trap. When fimbriae are stretched by controlling the movement of a piezoelectric stage, the bead is displaced at a distance (d) from the center of the trap. The predefined distance d corresponds to stretching force F on type 3 fimbriae. The stretching procedure stops when all fimbriae detach in turn from the bead.

kept at 4°C for later use. No interaction was observed between beads without antibody coating and bacteria expressing type 3 fimbriae. Coverslips were thoroughly rinsed with deionized water, dried completely, and then placed onto a rack before use.

Two coverslips were spaced ~170 μm apart by means of two layers of double-sided tape. Next, 40 μl of freshly resuspended *E. coli* in PBS was injected into the space between the two coverslips, left undisturbed for 1 min before the PBS solution in the space was completely removed with filter paper, and then left for 30 min to ensure the immobilization of bacteria on the bottom coverslip. Subsequently, 40 μl of surface-modified beads in PBS was meticulously injected into the space. Finally, the sample was immediately placed into the sample holder and left for 1 h to ensure again the adhesion of most bacteria to the bottom coverslip before elasticity measurements.

The OT setup used in this study has been described elsewhere (10, 11) and is schematically shown in Fig. 2A. The setup details are listed in Table S1 in the supplemental material. Basically, a trapping laser beam and a probing laser beam were guided into an inverted microscope and then passed through a high-numerical-aperture objective to form two diffraction-limited focal points on a sample. The trapping laser was then used to capture a bead. The probing laser was used to detect force-dependent displacement of the trapped bead.

For the calibration of our OT, the light of the probing laser scattered by the trapped particle was collected by a condenser and the scattering pattern on the back focal plane of the condenser was then imaged on a quadrant photodiode. Next, voltage output signals from the quadrant photodiode were increased by an electronic amplifier with a 1-kHz low-pass filter and sampled at 10 kHz with a data acquisition card in a personal computer. Finally, the stiffness, also known as the spring constant, of the trapping force imposed on the trapped particle was derived from an analysis of voltage signals by using a modification of the power spectral density method with Faxén's law (4).

Measurement procedure in our OT system. The immobilization of bacteria, as depicted in the diagram of our elasticity measurement processes (Fig. 2B), is different from that in previous studies of type 1 fimbriae or P fimbriae with OT (2, 24). In this study, to avoid possible optical damage to the bacteria, they were immobilized directly on the bottom coverslip rather than being mounted on a big bead to indirectly immobilize them to the bottom coverslip. Next, a 1-μm, surface-modified bead was trapped for calibration by the power spectral density method (4). The stiffness of the trapping force on the bead was typically 750 pN/μm. The effective maximum of the trapping force was smaller than 180 pN. Then, the calibrated bead was moved near a bacterium, and we waited for adhesion of some type 3 fimbriae to the bead. Finally, the movement of the bacterium at a pulling speed of 0.01 or 0.05 μm/s by a piezo electric stage resulted in the gradual extension of type 3 fimbriae between the trapped bead and the bacterium.

RESULTS

Morphology of the type 3 fimbria-expressing bacteria. A TEM image of the recombinant *E. coli* strain expressing type 3 fimbriae is shown in Fig. 3A. We estimated the average density and the unstretched lengths, two structural parameters of type 3 fimbriae expressed on a bacterium. Typically, a recombinant *E. coli* bacterium expresses approximately 1,800 fimbriae (12 bacteria) and each fimbria has a length ranging from 0.8 to 2.1 μm (209 fimbriae). The average unstretched length of fimbriae is 1.5 ± 0.4 μm. As a whole, type 3 fimbriae deposited on a solid substrate often appear tangled together in bundles. In addition, the backbone of a type 3 fimbria seems curved rather than straight.

Structural parameters of the type 3 fimbriae, namely, pitch and varied widths. In the TEM images with a high magnification, fimbriae with striations presumably derived from the major assembling subunit MrkA are clearly visible. Every interval between two striations is called pitch (Δh, where h is the length of a fimbria). Overall, the estimated pitches were shown to be similar values, for example, 4.3 nm (Fig. 3B) and 3.9 nm (Fig. 3C). After considerable measurements and data analysis, a frequency histogram for the pitch was plotted (Fig. 3D). The Gaussian fit gave an average pitch of 4.1 nm (standard deviation [SD], 0.4) (n = 5,060; 506 fimbriae).

In general, the widths of fimbriae examined in the TEM images were measured along their backbones and were approximately 7 nm (Fig. 3B and C). A frequency histogram for the width of fimbriae was created (Fig. 3E). The Gaussian fit gave an average width of 7.4 nm (SD, 0.8) (n = 6,909; 506 fimbriae). Nevertheless, some fimbriae showed continuously varied widths ranging between 3.8 and 7.5 nm (for example, the right part of Fig. 3C). The smallest widths were almost found between two adjacent segments of a fimbria, and the segments gradually widened away from the smallest widths (for example, the left part of Fig. 3C). After some of the smallest widths on cracked segments of fimbriae were excluded, a frequency histogram for the smallest widths was created (Fig. 3F). The Gaussian fit gave an average width of 4.2 nm (SD, 0.5) (n = 480; 272 fimbriae).

Young's moduli derived from two persistence lengths. To confirm that the estimated Young's moduli are independent of the choice of two contour lengths, a TEM image for estimating two kinds of persistence lengths of type 3 fimbriae is shown in Fig. 4A. For the contour length of 1,935 Å, two estimated end-to-end distances were 1,901 and 1,907 Å (Fig. 4A). For the contour length of 3,010 Å, one estimated end-to-end distance was 2,901 Å (Fig. 4A). A frequency histogram for the first kind of end-to-end distances is shown in Fig. 4B. An expected value for the end-to-end distance was estimated at 1,909 Å (n = 998; 506 fimbriae), and the corresponding persistence length was 1.127 μm. A frequency histogram for the second kind of end-to-end distances is shown in Fig. 4C. An expected value

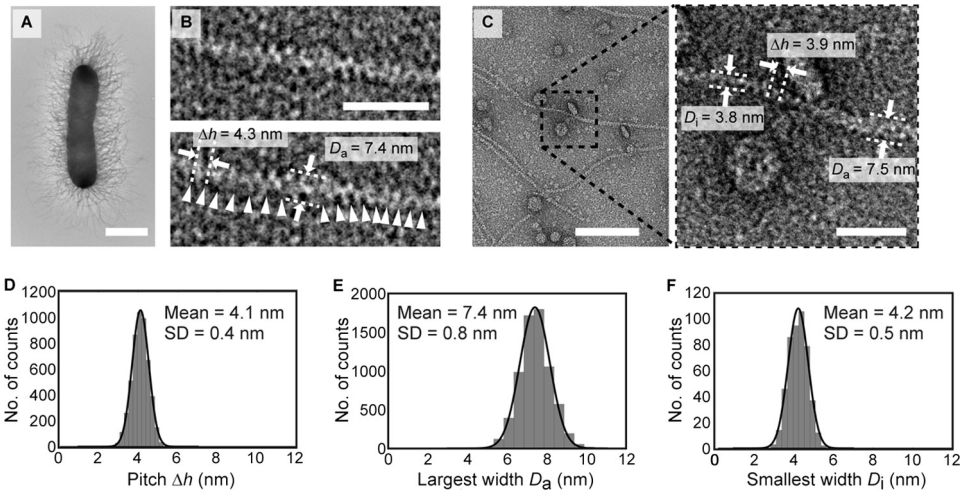

FIG. 3. (A) TEM image of JM109(p*mrkABCD*). The density of type 3 fimbriae expressed on the bacterium is ~1,800 fimbriae per bacterium ($n = 12$), and the unstretched lengths of fimbriae average 1.5 μm (SD, 0.4) ($n = 209$ fimbriae). (B) TEM images for estimating the pitch and largest width. The upper part is an undecorated image of a type 3 fimbria. The lower part has striation-indicated arrowheads periodically lined on the side of the same fimbria from the upper part. (C) TEM image for estimating the pitch and the largest and smallest widths. The right part is an enlargement of the square frame from the left part. (D) Frequency histogram for the pitch, Δh. Gaussian fit analysis gave an average pitch of 4.1 nm (SD, 0.4) ($n = 5{,}060$; 506 fimbriae). (E) Frequency histogram for the largest width (D_a). Gaussian fit analysis gave an average width of 7.4 nm (SD, 0.8) ($n = 6{,}909$; 506 fimbriae). (F) Frequency histogram for the smallest width (D_i). Gaussian fit analysis gave an average width of 4.2 nm (SD, 0.5) ($n = 480$; 272 fimbriae). The scale bars in panel A, panel B, and the left and right parts of panel C are 2 μm, 25 nm, 100 nm, and 25 nm, respectively.

for the end-to-end distance was estimated at 2,958 Å ($n = 428$; 415 fimbriae), and the corresponding persistence length was 1.369 μm.

After data analysis and then placement of two estimated persistence lengths (P) into equation 2, the estimated Young's moduli (E) were 98 MPa for the contour length of 1,935 Å and 120 MPa for the contour length of 3,010 Å. It seems that two estimated Young's moduli are almost independent of the choice of contour lengths.

Force-extension curve of type 1 fimbriae. In order to confirm our experimental finding about the mechanical properties of type 3 fimbriae, we reproduced the FEC of well-studied type 1 fimbriae, as shown in Fig. S1 and Movie S1 in the supplemental material. The average uncoiling force was 33.5 pN (SD, 0.1) ($n = 2$), and the characteristic force was 64.2 pN ($n = 1$). Both of the results are consistent with the published data (2).

Force-extension curve of a single stretched type 3 fimbria. Most of our initial elasticity measurements (~1,000 stretching events) were not successful primarily due to attachments of multiple fimbriae to a trapped bead. The resulting elastic force of the fimbriae was eventually larger than the trapping force and led to the separation of an OT-trapped bead from the trap. Nevertheless, an operated process was used to decrease the number of attached fimbriae to the trapped bead. By a fixed separation of the trap from the OT-trapped bead, a moderate trapping force could be steadily applied to the attached fimbriae, suppressing the fimbrial attachments to the bead. After this process, some individually trapped beads remained attached to a few fimbriae ($n = 19$), as shown in Movie S2 in the supplemental material. In addition, some FECs fortunately involved the attachment of only one type 3 fimbria to a bead ($n = 3$).

In Fig. 5, a solid, black curve depicts a typical FEC of a single type 3 fimbria. The FEC is divided into three phases: the first nonlinear phase (phase I), the uncoiling phase (phase II), and the final nonlinear phase (phase III). Except in the first nonlinear phase, the FEC of type 3 fimbriae is qualitatively similar to the FEC of a type 1 fimbria or a P fimbria.

In the first nonlinear phase, a type 3 fimbria is stretched nonlinearly with increasing force. When approaching the uncoiling phase, the extension of the type 3 fimbria approximates a Hooke's spring. The gray × curve in Fig. 5 displays the corresponding spring constant-extension curve of the fimbria. The maximum spring constant, k_p, of 261.8 pN/μm occurs in this phase. Next, as the stretching force reaches the uncoiling force, the extension of the type 3 fimbria dramatically switches to the uncoiling phase. In the uncoiling phase, the fimbria continues to stretch at a stable uncoiling force of 70.1 pN, with notable fluctuations due to the uncoiling of its helical structure in turn. After the uncoiling phase, the FEC of the fimbria has an inclined S shape with an inflection point, at which the characteristic force is 116.4 pN. Past the inflection point, the stretching force rapidly increases over a few hundred piconewtons.

Young's modulus derived from a spring constant. According to the theory of mechanics, the elasticity of type 3 fimbriae for one-dimensional deformation is characterized by Young's modulus E (in units of N/m^2) as given by

$$E = \frac{F \times l}{A \times \Delta l} = \frac{k_p \times l}{\pi(D_a \times D_i/4)} \quad (3)$$

where F (N) is the stretching force to the fimbria, A (m^2) is the cross area of the fimbria, D_a (m) and D_i (m) are diameters of elliptic cross sections of the fimbria, l (m) is the unstretched length of the fimbria, Δl (m) is the extension of the fimbria, and k_p (N/m) is the spring constant of the fimbria.

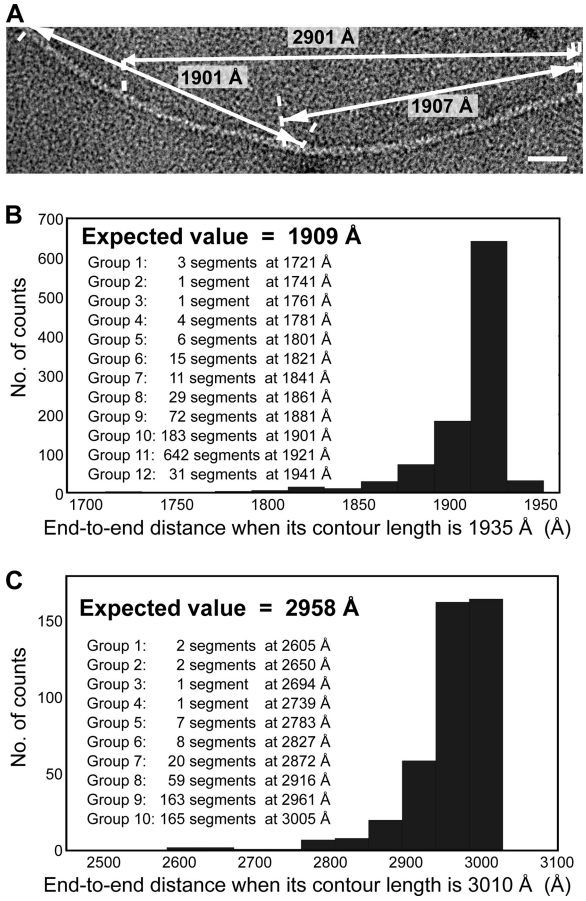

FIG. 4. (A) TEM image for estimating two kinds of end-to-end distances of a type 3 fimbria. The scale bar is 250 Å. (B) Frequency histogram for end-to-end distances when their contour length is 1,935 Å. The number of groups is 12. An expected value for the end-to-end distance was estimated at 1,909 Å (n = 998; 506 fimbriae). (C) Frequency histogram for end-to-end distances when their contour length is 3,010 Å. The number of groups is 10. An expected value for the end-to-end distance was estimated at 2,958 Å (n = 428; 415 fimbriae).

With reference to the single type 3 fimbria depicted in Fig. 5 and some structural parameters, substituting the appropriate values ($k_p \cong 261.8$ pN/μm, $l = 1.53$ μm, $D_a = 7.4$ nm, and $D_i = 4.2$ nm) into equation 3 for E results in a maximum estimation

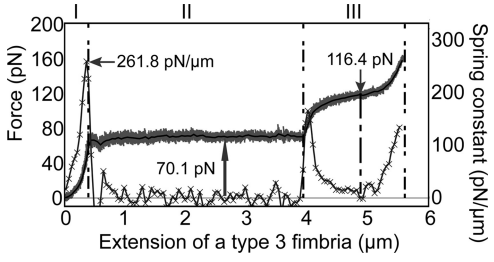

FIG. 5. Typical force-extension curve of a single type 3 fimbria is represented by the solid, black curve. The uncoiling force in phase II is 70.1 pN (upward-pointing arrow). The characteristic force at the inflection point marked with a downward-pointing arrow is 116.4 pN. In addition, a typical spring constant-extension curve of a single type 3 fimbria is represented by the gray × curve. The maximum spring constant in phase I is 261.8 pN/μm (leftward-pointing arrow).

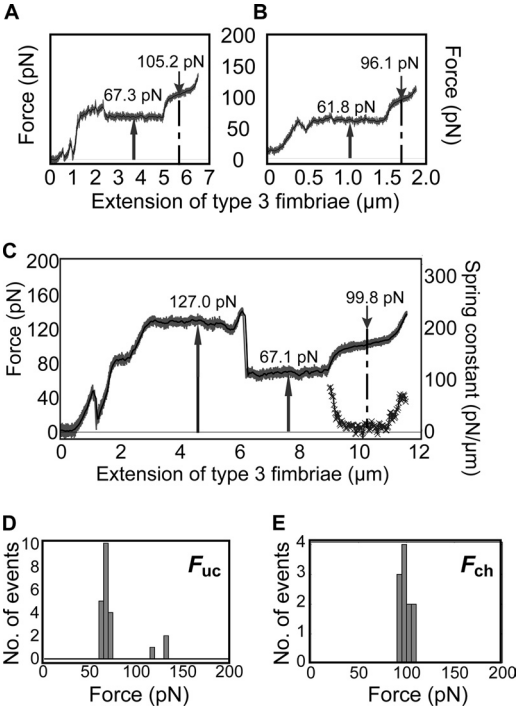

FIG. 6. (A and B) Force-extension curves of single type 3 fimbriae. The uncoiling force is 67.3 pN and the characteristic force is 105.2 pN (arrows) in panel A. The uncoiling force is 61.8 pN and the characteristic force is 96.1 pN in panel B. (C) Force-extension curve of type 3 fimbriae with a stepwise uncoiling is represented by the solid, black curve. After the extension of 3 μm, the force level of uncoiling forces decreases from 127.0 to 67.1 pN step by step. In addition, a typical spring constant-extension curve of the fimbriae is represented by the gray, × curve, and the characteristic force is 99.8 pN at the inflection point, with a minimum spring constant. (D) Frequency histogram for the uncoiling force, F_{uc}. Two groups of uncoiling forces can be distinguished and mediated the binding during the uncoiling of one fimbria and simultaneous uncoiling of two fimbriae, respectively. The average values of the uncoiling forces in two groups were estimated at 66.8 pN (SD, 3.6) (n = 19; 19 fimbriae) and 124.1 pN (SD, 8.8) (n = 3; 3 fimbriae), respectively. Statistically, the uncoiling forces of single type 3 fimbriae have an average of 66.2 pN (SD, 4.0). (E) Frequency histogram for the characteristic force, F_{ch}. The characteristic forces have an average of 101.9 pN (SD, 8.6) (n = 14; 14 fimbriae).

of Young's modulus of 16.4 MPa in the first nonlinear phase. Statistically, the average estimated Young's modulus was 15.7 MPa (SD, 2.3) (n = 3).

Assessment of the uncoiling force. In the uncoiling phase, the measured uncoiling forces of type 3 fimbriae were similar at 0.01 μm/s or at 0.05 μm/s in pulling speed. It suggested that all experiments were operated under steady-state conditions. The typical FECs of single type 3 fimbriae are shown in Fig. 6A and B, with uncoiling forces of 67.3 pN and 61.8 pN for two different fimbriae, respectively. In addition, the other typical FEC shows an extension of a stepwise uncoiling mechanism as long as nearly 9 μm in the uncoiling phase, as shown in Fig. 6C. Note that in the uncoiling phase after the extension of 3 μm, the force level of uncoiling forces decreases from 127.0 pN to 67.1 pN step by step. This corresponds to binding with two type 3 fimbriae, which uncoiled simultaneously and then sequen-

tially detached from the trapped bead with the increasing bacterium-to-bead distance.

The uncoiling forces derived from the uncoiling phase in all elasticity measurements were evaluated and plotted as a frequency histogram. As shown in Fig. 6D, two groups of uncoiling forces mediate the binding of one fimbria and two fimbriae to a bead, respectively. The average values of the uncoiling forces in two groups were estimated to be 66.8 pN (SD, 3.6) (n = 19; 19 fimbriae) and 124.1 pN (SD, 8.8) (n = 3; 3 fimbriae), respectively. We supposed that the two groups represented binding events meditated by one fimbria and by two fimbriae in their uncoiling phase, respectively. In other words, according to the lowest common multiple of measured uncoiling forces, the uncoiling forces averaged 66.2 pN (SD, 4.0) (n = 22, 20 fimbriae) in steady state.

Assessment of the characteristic force. In the final nonlinear phase, the characteristic force of type 3 fimbriae was determined. The two characteristic forces were 105.2 pN and 96.1 pN for two different single fimbriae, as shown in Fig. 6A and B, respectively. In addition, although Fig. 6C shows the binding of two fimbriae to a trapped bead, we found a characteristic force of 99.8 pN. This actually shows that only one fimbria was stretched under its final nonlinear phase until one of two fimbriae detached from the bead. The characteristic forces were measured and plotted as a frequency histogram. As shown in Fig. 6E, the characteristic forces averaged 101.9 pN (SD, 8.6) (n = 14; 14 fimbriae).

DISCUSSION

Flexibility and ellipse-like cross section of a type 3 fimbria. With respect to fimbrial structure, two interesting features of type 3 fimbriae are proposed as follows. First, we found that type 3 fimbriae seem to be curved due to flexibility (Fig. 3A). We have characterized the flexibility of type 3 fimbriae by persistence length. The estimated persistence length was approximately 1 μm. According to the theory of elasticity, shorter persistence lengths are related to more flexible structures. In contrast, the persistence lengths of P fimbriae were estimated to be in the range of 1 to 8 μm (5). This suggests that type 3 fimbriae are more flexible than P fimbriae.

Second, as shown in Fig. 3C, the varied widths of a fimbria along its backbone are supposed to indicate that the fimbria might be merely twisted by bacterial secretions rather than by shrinkage due to electron beams. The direct evidence showed that the pitch of the segment with varied widths remained visible and almost the same. In addition, the twist of type 3 fimbriae should be infrequent and passive, since only a few segments of some fimbriae exhibited continuously varied widths. The twists of type 3 fimbriae were different from the frequent twists of two strands in cylindrical F-actin filaments (15). Furthermore, the twist of well-studied cylindrical structures of type 1 fimbriae and P fimbriae was not found (19, 30). Possibly, type 3 fimbriae have had an elliptically cylindrical structure. Largest width and smallest width can be regarded as the largest diameter and smallest diameter of each ellipse-like cross section in fimbrial structures. Statistically, the largest diameter was 7.4 nm and the smallest was 4.2 nm. Our estimated diameters of type 3 fimbriae are in agreement with published data that reported a range from 4 nm to 5 nm (14). Recently, an initial model in the three-dimensional reconstitution of type 3 fimbriae also exhibited ellipse-like cross sections (data not shown).

Characterization of three stretched phases of single type 3 fimbriae. Structurally, the pitch of type 3 fimbriae suggests that the fimbriae have helix-like structures, indicating that the fimbriae could be uncoiled and stretched. Similarly, in studies of the elasticity of type 3 fimbriae, we have confirmed that type 3 fimbriae exhibit extension in three phases: the first nonlinear phase, the uncoiling phase, and the final nonlinear phase. Figure 5 represents the typical FEC of a single type 3 fimbria. Remarkably, the uncoiling forces in Fig. 6D were classified by two groups whose average values were 67 and 124 pN, respectively. The latter value is nearly double the former. In addition, we never found any intermediate value for uncoiling forces at 30, 90, or 150 pN. Statistically, the uncoiling force of type 3 fimbriae is 66 pN and similar to that in Fig. 5.

After determination of the typical FEC of an individual fimbria, the extension of the fimbria in three phases was further examined. The stretched behavior of the fimbria in the first phase was found to be nonlinear in elasticity measurements. Owing to the curved nature of type 3 fimbriae, the backbone of a stretched fimbria has to be first changed from curved to straight. In addition, the nonlinearly stretched behavior of a curved DNA (7) or a curved flagellum (13) has been demonstrated. Therefore, it is possible that the stretched behavior of a fimbria in the first phase is possibly nonlinear rather than linear like the extension of a Hooke's spring. Nevertheless, a worm-like chain model (7), which well describes the nonlinear elasticity of DNA, is invalid for type 3 fimbriae since the persistence length of fimbriae is not shorter than the unstretched lengths of fimbriae. A refined model to describe the first nonlinear extension behavior of type 3 fimbriae remains to be done.

As for the later two phases, a sticky-chain model, which describes the stretched behaviors of a type 1 fimbria or a P fimbria (1, 23), is suitable to describe the later two phases of a type 3 fimbria. Conceptually, in the uncoiling phase, closed layer-to-layer (LL) bonds in the helix-like structure of a type 3 fimbria are opened successively with the uncoiling force of 66 pN. The magnitude of the uncoiling force is generally regarded as a key feature of fimbriae. However, according to dynamic force spectroscopy experiments on P fimbriae and type 1 fimbriae (2), the uncoiling force depends on the extension speed. In the final nonlinear phase, all LL bonds are open, but closed head-to-tail (HT) bonds are opened independently rather than successively like the LL bonds. Furthermore, the probability of opening individual HT bonds is largest at the characteristic force of 102 pN. Therefore, regardless of the length of the fimbria, the extension of the fimbria in the third phase is largest as a stretching force approaches the characteristic force. Furthermore, since the characteristic forces of three types of fimbriae are fixed and independent of an extension speed, we advise that the characteristic force be regarded as an alternative feature for recognizing the type of fimbriae.

Comparison of type 3 fimbriae with P fimbriae and type 1 fimbriae. Three structural parameters and three mechanical parameters of type 3 fimbriae, characterized in our experiments, and of type 1 fimbriae and P fimbriae, cited from published reports, are summarized in Table 1. Compared with type

TABLE 1. Structural and mechanical parameters of type 3 fimbriae, type 1 fimbriae, and P fimbriae

Fimbria type	Structural parameters			Mechanical parameters		
	Pitch (nm)	Cross section (nm by nm)	Unstretched length (μm)	Young's modulus (MPa)	Uncoiling force (pN)	Characteristic force (pN)
Type 3	4.1	π by 7.4 by 4.2 (ellipse-like)	1.5	100[d] or 16[e]	66	102
Type 1[a]	2.41	π by 6.9 by 6.9 (spherical)	~1	100[c]	30	67
P[b]	2.47	π by 8.2 by 8.2[c] (spherical)	0.3–1.5	50–400[d] or 4[e]	28	67

[a] For the physical parameters of type 1 fimbriae, see references 2, 17, 19, and 29.
[b] For the physical parameters of P fimbriae, see references 2, 6, 24, and 30.
[c] A filament diameter is 6.8 nm, with surface protrusions that extend 0.7 nm from the filament surface.
[d] The values are estimated from persistence lengths.
[e] The values are estimated from elasticity experiments.

1 fimbriae and P fimbriae, type 3 fimbriae have two similar parameters, unstretched length and Young's modulus. We found that, for both type 3 fimbriae and P fimbriae, the Young's moduli derived from their spring constants are remarkably smaller than those derived from their persistence lengths. According to an elasticity experiment on DNA, a typical model of polymers, the nature of Young's modulus of DNA appears in the later and linear region of a force-extension curve (44). Similarly, we expected that the Young's modulus of type 3 fimbriae could be estimated at a maximum extension in the first nonlinear phase. Furthermore, the estimated Young's modulus from a maximum spring constant in the first nonlinear phase might be as large as that from the persistence length. However, the smaller Young's modulus derived from a spring constant suggested that individual fimbriae might not be fully stretched to exhibit the nature of Young's modulus since the stretching force started to uncoil the helical structures of the fimbriae and made them enter their second phases.

Conversely, four other parameters of type 3 fimbriae are different from those of type 1 fimbriae and P fimbriae. Among the different parameters, the pitch and the uncoiling force as well as the characteristic force are further discussed below. First, compared with the other two types of fimbriae, the larger pitches in the helix-like structures of type 3 fimbriae could result from the higher molecular weights of the major subunits, pilins. From the amino acid compositions of three types of pilins (3, 18, 25) and the volumes occupied by amino acids in the pilins (20), we estimated that the densities of three types of pilins are similar and approximately 0.81 Da/Å^3. The occupied volume of the pilins in type 3 fimbriae should be larger, because the pilins have higher molecular weights. Therefore, the pitches in the helix-like structures of type 3 fimbriae are certainly larger. Second, type 3 fimbriae had stronger uncoiling and characteristic force. This implies that the mechanical impact of flushes on type 3 fimbriae could be larger than on P fimbriae and type 1 fimbriae.

Biological relevance. In this study, the uncoiling force of type 3 fimbriae was confirmed. The *E. coli* strains expressing P fimbriae are most frequently associated with infections in the upper urinary tract and kidney that cause pyelonephritis, whereas *E. coli* strains expressing type 1 fimbriae are found in the lower urinary tract and bladder to cause cystitis (27, 36, 45). The difference in uncoiling forces between P fimbriae and type 1 fimbriae has been attributed to the fact that uropathogenic *E. coli* strains survive in the upper and lower urinary tracts (2). Type 1 fimbriae with stronger uncoiling forces have evolved to support higher flushing forces at shorter-time events, originating from the irregular urine flow in the bladder compared with the constant urine flow in the upper urinary tract. It is suggested that in different host environments, some mechanical impacts affect the type of fimbriae expressed on bacteria. Although type 3 fimbriae are regarded to have a major role in biofilm formation (31), a recent report still failed to associate the expression of type 3 fimbriae with lung or urinary tract infection in the mouse model (39). Moreover, the receptor of type 3 fimbriae has not yet been identified. Whether the relatively strong uncoiling force of type 3 fimbriae plays a role in providing for detachment from collagen-rich organs remains to be investigated.

ACKNOWLEDGMENTS

We thank Der-San Chuu and Sien Chi at National Chiao Tung University for valuable discussions, Wen-Hsiung Ko at National Chung Hsing University for writing suggestions, Chung-Shi Yang at the National Health Research Institutes for kindly providing a Hitachi-H7650 EM to generate the preliminary results, the Institute of Molecular Biology, Academia Sinica, for kindly providing an FEI Tecnai G^2 EM to be used, Wei-Hau Chang at the Academia Sinica for kindly providing a Zeiss imaging scanner for TEM image digitalization, Yu-Ching Chen and Shu-Ping Tasi for EM technical assistance, and Meng-Yen Ku for collecting elasticity data for fimbriae.

This work was supported by grants 94-2120-M009-015, 95-2120-M-009-005, and 96-2120-M-009-003 from the 2005-2007 National Research Program for Nanoscience and Technology, National Science Council, Taiwan, Republic of China. Economic support from National Chiao Tung University enabled improvement in our optical-tweezers system.

REFERENCES

1. **Andersson, M., E. Fällman, B. E. Uhlin, and O. Axner.** 2006. A sticky chain model of the elongation and unfolding of *Escherichia coli* P pili under stress. Biophys. J. **90:**1521–1534.
2. **Andersson, M., B. E. Uhlin, and E. Fällman.** 2007. The biomechanical properties of *E. coli* pili for urinary tract attachment reflect the host environment. Biophys. J. **93:**3008–3014.
3. **Baga, M., et al.** 1984. Nucleotide sequence of the *papA* gene encoding the Pap pilus subunit of human uropathogenic *Escherichia coli*. J. Bacteriol. **157:**330–333.
4. **Berg-Sørensen, K., and H. Flyvbjerg.** 2004. Power spectrum analysis for optical tweezers. Rev. Sci. Instrum. **75:**594–612.
5. **Bullitt, E., and L. Makowski.** 1998. Bacterial adhesion pili are heterologous assemblies of similar subunits. Biophys. J. **74:**623–632.
6. **Bullitt, E., and L. Makowski.** 1995. Structural polymorphism of bacterial adhesion pili. Nature **373:**164–167.
7. **Bustamante, C., J. F. Marko, E. D. Siggia, and S. Smith.** 1994. Entropic elasticity of lambda-phage DNA. Science **265:**1599–1600.
8. **Castelain, M., et al.** 2009. Characterization of the biomechanical properties of T4 pili expressed by *Streptococcus pneumoniae*—a comparison between helix-like and open coil-like pili. Chemphyschem **10:**1533–1540.

9. **Castelain, M., A. Sjöström, E. Fällman, B. Uhlin, and M. Andersson.** 2010. Unfolding and refolding properties of S pili on extraintestinal pathogenic *Escherichia coli*. Eur. Biophys. J. **39:**1105–1115.
10. **Chang, B. J., et al.** 2006. Measurement of the adhesive force between a single *Klebsiella pneumoniae* type 3 fimbria and collagen IV using optical tweezers. Biochem. Biophys. Res. Commun. **350:**33–38.
11. **Chen, F. J., et al.** 2007. Uncoiling mechanism of *Klebsiella pneumoniae* type 3 pili measured by using optical tweezers. Presented at the Conference on Optical Trapping and Optical Micromanipulation IV, San Diego, CA, 26 to 29 August 2007. Proc. SPIE 6644, 66441W. doi:10.1117/12.733097.
12. **Choudhury, D., et al.** 1999. X-ray structure of the FimC-FimH chaperone-adhesin complex from uropathogenic *Escherichia coli*. Science **285:**1061–1066.
13. **Darnton, N. C., and H. C. Berg.** 2007. Force-extension measurements on bacterial flagella: triggering polymorphic transformations. Biophys. J. **92:**2230–2236.
14. **Duguid, J. P.** 1959. Fimbriae and adhesive properties in *Klebsiella* strains. J. Gen. Microbiol. **21:**271–286.
15. **Egelman, E. H., N. Francis, and D. J. DeRosier.** 1982. F-actin is a helix with a random variable twist. Nature **298:**131–135.
16. **Fällman, E., S. Schedin, J. Jass, B. E. Uhlin, and O. Axner.** 2005. The unfolding of the P pili quaternary structure by stretching is reversible, not plastic. EMBO Rep. **6:**52–56.
17. **Forero, M., O. Yakovenko, E. V. Sokurenko, W. E. Thomas, and V. Vogel.** 2006. Uncoiling mechanics of *Escherichia coli* type I fimbriae are optimized for catch bonds. PLoS Biol. **4:**1509–1516.
18. **Gerlach, G. F., B. L. Allen, and S. Clegg.** 1988. Molecular characterization of the type 3 (MR/K) fimbriae of *Klebsiella pneumoniae*. J. Bacteriol. **170:**3547–3553.
19. **Hahn, E., et al.** 2002. Exploring the 3D molecular architecture of *Escherichia coli* type 1 pili. J. Mol. Biol. **323:**845–857.
20. **Harpaz, Y., M. Gerstein, and C. Chothia.** 1994. Volume changes on protein folding. Structure **2:**641–649.
21. **Hornick, D. B., B. L. Allen, M. A. Horn, and S. Clegg.** 1992. Adherence to respiratory epithelia by recombinant *Escherichia coli* expressing *Klebsiella pneumoniae* type 3 fimbrial gene products. Infect. Immun. **60:**1577–1588.
22. **Huang, Y. J., C. C. Wu, M. C. Chen, C. P. Fung, and H. L. Peng.** 2006. Characterization of the type 3 fimbriae with different MrkD adhesins: possible role of the MrkD containing an RGD motif. Biochem. Biophys. Res. Commun. **350:**537–542.
23. **Jäger, I. L.** 2001. The "sticky chain": a kinetic model for the deformation of biological macromolecules. Biophys. J. **81:**1897–1906.
24. **Jass, J., et al.** 2004. Physical properties of *Escherichia coli* P pili measured by optical tweezers. Biophys. J. **87:**4271–4283.
25. **Klemm, P.** 1984. The *fimA* gene encoding the type-1 fimbrial subunit of *Escherichia coli*: nucleotide sequence and primary structure of the protein. Eur. J. Biochem. **143:**395–399.
26. **Kline, K. A., S. Falker, S. Dahlberg, S. Normark, and B. Henriques-Normark.** 2009. Bacterial adhesins in host-microbe interactions. Cell Host Microbe **5:**580–592.
27. **Lane, M. C., and H. L. T. Mobley.** 2007. Role of P-fimbrial-mediated adherence in pyelonephritis and persistence of uropathogenic *Escherichia coli* (UPEC) in the mammalian kidney. Kidney Int. **72:**19–25.
28. **Liou, G. G., J. C. Tanny, R. G. Kruger, T. Walz, and D. Moazed.** 2005. Assembly of the SIR complex and its regulation by O-acetyl-ADP-ribose, a product of NAD-dependent histone deacetylation. Cell **121:**515–527.
29. **Miller, E., T. Garcia, S. Hultgren, and A. F. Oberhauser.** 2006. The mechanical properties of *E. coli* type 1 pili measured by atomic force microscopy techniques. Biophys. J. **91:**3848–3856.
30. **Mu, X. Q., and E. Bullitt.** 2006. Structure and assembly of P-pili: a protruding hinge region used for assembly of a bacterial adhesion filament. Proc. Natl. Acad. Sci. U. S. A. **103:**9861–9866.
31. **Ong, C. L. Y., et al.** 2008. Identification of type 3 fimbriae in uropathogenic *Escherichia coli* reveals a role in biofilm formation. J. Bacteriol. **190:**1054–1063.
32. **Reif, F.** 1965. Fundamentals of statistical and thermal physics. McGraw-Hill, New York, NY.
33. **Rivetti, C., M. Guthold, and C. Bustamante.** 1996. Scanning force microscopy of DNA deposited onto mica: equilibration versus kinetic trapping studied by statistical polymer chain analysis. J. Mol. Biol. **264:**919–932.
34. **Sauer, F. G., et al.** 2000. Chaperone-assisted pilus assembly and bacterial attachment. Curr. Opin. Struct. Biol. **10:**548–556.
35. **Sauer, F. G., H. Remaut, S. J. Hultgren, and G. Waksman.** 2004. Fiber assembly by the chaperone-usher pathway. Biochim. Biophys. Acta Mol. Cell Res. **1694:**259–267.
36. **Schilling, J. D., M. A. Mulvey, and S. J. Hultgren.** 2001. Structure and function of *Escherichia coli* type 1 pili: new insight into the pathogenesis of urinary tract infections. J. Infect. Dis. **183:**S36–S40.
37. **Snyder, J. A., et al.** 2005. Coordinate expression of fimbriae in uropathogenic *Escherichia coli*. Infect. Immun. **73:**7588–7596.
38. **Soto, G. E., and S. J. Hultgren.** 1999. Bacterial adhesins: common themes and variations in architecture and assembly. J. Bacteriol. **181:**1059–1071.
39. **Struve, C., M. Bojer, and K. A. Krogfelt.** 2009. Identification of a conserved chromosomal region encoding *Klebsiella pneumoniae* type 1 and type 3 fimbriae and assessment of the role of fimbriae in pathogenicity. Infect. Immun. **77:**5016–5024.
40. **Tarkkanen, A. M., et al.** 1990. Type V collagen as the target for type-3 fimbriae, enterobacterial adherence organelles. Mol. Microbiol. **4:**1353–1361.
41. **Tarkkanen, A. M., R. Virkola, S. Clegg, and T. K. Korhonen.** 1997. Binding of the type 3 fimbriae of *Klebsiella pneumoniae* to human endothelial and urinary bladder cells. Infect. Immun. **65:**1546–1549.
42. **Thomas, W. E., L. M. Nilsson, M. Forero, E. V. Sokurenko, and V. Vogel.** 2004. Shear-dependent 'stick-and-roll' adhesion of type 1 fimbriated *Escherichia coli*. Mol. Microbiol. **53:**1545–1557.
43. **Tsai, F. C., Y. T. Huang, L. Y. Chang, and J. T. Wang.** 2008. Pyogenic liver abscess as endemic disease, Taiwan. Emerg. Infect. Dis. **14:**1592–1600.
44. **Wang, M. D., H. Yin, R. Landick, J. Gelles, and S. M. Block.** 1997. Stretching DNA with optical tweezers. Biophys. J. **72:**1335–1346.
45. **Wullt, B., et al.** 2001. P-fimbriae trigger mucosal responses to *Escherichia coli* in the human urinary tract. Cell. Microbiol. **3:**255–264.